Chemical Science

ROYAL SOCIETY OF CHEMISTRY

EDGE ARTICLE

View Article Online
View Journal | View Issue

Cite this: *Chem. Sci.*, 2020, **11**, 3687

All publication charges for this article have been paid for by the Royal Society of Chemistry

Effects of sedimentation, microgravity, hydrodynamic mixing and air–water interface on α-synuclein amyloid formation†

Jiangtao Zhou,‡[a] Francesco S. Ruggeri,‡*[bc] Manuela R. Zimmermann,[b] Georg Meisl,[b] Giovanni Longo,[d] Sergey K. Sekatskii,[a] Tuomas P. J. Knowles *[bc] and Giovanni Dietler *[a]

The formation of amyloid fibrils is a characterizing feature of a range of protein misfolding diseases, including Parkinson's disease. The propensity of native proteins to form such amyloid fibril, both *in vitro* and *in vivo*, is highly sensitive to the surrounding environment, which can alter the aggregation kinetics and fibrillization mechanisms. Here, we investigate systematically the influence of several representative environmental stimuli on α-synuclein aggregation, including hydrodynamic mixing, the presence of an air–water interface and sedimentation. Our results show that hydrodynamic mixing and interfacial effects are critical in promoting several microscopic steps of α-synuclein aggregation and amyloid fibril formation. The presence of an air–water interface under agitation significantly promoted primary nucleation. Secondary processes were facilitated by hydrodynamic mixing, produced by 3D rotation and shaking either in the presence or in the absence of an air–water interface. Effects of sedimentation, as investigated in a microgravity incubator, of α-synuclein lead only to minor changes on the aggregation kinetics rates in comparison to static conditions. These results forward the understanding of α-synuclein fibrillization, paving the way for the development of high-throughput assays for the screening of pharmacological approaches targeting Parkinson's disease.

Received 15th January 2020
Accepted 6th March 2020

DOI: 10.1039/d0sc00281j

rsc.li/chemical-science

Introduction

The formation of pathological fibrillar amyloid aggregates is associated with several protein misfolding diseases, including many neurodegenerative disorders.[1–3] Within this class of diseases, Parkinson's diseases[4–6] is fundamentally linked at the molecular level with the misfolding and aggregation of the α-synuclein protein.

The mechanistic link between α-synuclein amyloid formation and disease onset is still elusive and to date no treatments to delay or cure Parkinson's disease are available. This knowledge gap in part originates in a lack of comprehensive understanding of the energy landscape and the kinetics of the transition from soluble native monomers to insoluble amyloid fibrils. Further limiting factors are related to the poor reproducibility of the kinetics of aggregation, as well as a high degree of polymorphism, which reflects on the weak tendency of α-synuclein to spontaneously aggregate *in vitro*. These effects hamper the accurate study of α-synuclein aggregation required for high-throughput for biotechnology and drug discovery purposes.[7,8]

The aggregation kinetics of α-synuclein is routinely accelerated by exploiting the effect of solution conditions or other external factors, including pH,[9] temperature[9] and ionic strength,[9–11] as well as seed aggregates,[9,12,13] nanoparticles[14] and lipid vesicles.[15] Moreover, a variety of hydrodynamic mixing approaches, including stirring,[9,16] shaking[17] and shearing[18] are employed. In particular, hydrodynamic mixing plays a critical role in protein aggregation[9,14,19] and it has been previously shown that the strength of the hydrodynamic flow may be critical for accelerating fibril formation.[9,20] Further fundamental but elusive factors, which have been shown to influence protein aggregation kinetics are the phenomena of sedimentation during incubation and the interaction with air–water interfaces.[9,17,19] The poorly controlled presence of hydrophobic interfaces can cause uncertainty and variability in the kinetics of aggregation, as well as a high degree of polymorphism.[19,21–25] Furthermore, many biological activities are gravity-dependent,[26] such as lipid membrane fluidity[27–29] and ion channels,[30] and it

[a]*Laboratory of Physics of Living Matter, École Polytechnique Fédérale de Lausanne (EPFL), CH-1015 Lausanne, Switzerland. E-mail: giovanni.dietler@epfl.ch*

[b]*Department of Chemistry, University of Cambridge, Lensfield Road, Cambridge CB2 1EW, UK*

[c]*Centre for Misfolding Diseases, Department of Chemistry, University of Cambridge, Lensfield Road, Cambridge CB2 1EW, UK*

[d]*Istituto di Struttura della Materia, CNR, Via del Fosso del Cavaliere 100, Roma, 00133, Italy*

† Electronic supplementary information (ESI) available. See DOI: 10.1039/d0sc00281j

‡ These authors contributed equally to this work.

has been reported that microgravity and hyper-gravity conditions with under/over-sedimentation effect can promote or hinder the aggregation process respectively.[31] However the gravitational influence on protein aggregation is still not fully understood[31,32] and the understanding of the combined phenomena of sedimentation, hydrodynamic mixing and interaction with air–water interfaces on protein aggregation remains elusive.

In the present work, we undertake a systematic characterization of α-synuclein aggregation in static, microgravity and orbital shaking condition to investigate and unravel the influence of sedimentation, hydrodynamic mixing and air–water interfaces on the microscopic steps of primary nucleation and secondary processes of α-synuclein aggregation. To characterize the process of aggregation, we exploited a combination of Thioflavin T (ThT) based kinetics assays,[7,15,33] circular dichroism (CD) spectroscopy,[7,34] high-resolution atomic force microscopy (AFM) imaging[7,35,36] and the theoretical platform offered by chemical kinetics.[37,38]

Results and discussion

We selected six distinct conditions to study the influence of sedimentation, hydrodynamic mixing and the presence of an air–water interface on the aggregation of α-synuclein, as shown in Fig. 1 left. The protein solution was studied in three different dynamic conditions: (1) static; (2) orbital shaking, achieved by shaking at 400 rpm (rotations per minute) on a circular orbit on the horizontal plane; (3) microgravity environment, implemented by using a random position machine (RPM) with a 3D-linostat configuration, rotating at ~30 rpm.[29,39] Additionally, for each dynamic condition, the protein solution was sealed and incubated either in an Eppendorf tube in the presence of an air–water interface or in a syringe in the absence of any air–water interface. The experiments were performed at pH 7.4, at 37 °C and at a variable initial monomeric concentration between 20 and 65 μM. Aliquots were taken at different time points and characterized by AFM, CD and ThT assays.

In the static syringe (static-Syr), the aggregation was subject only to sedimentation effects, while in the Eppendorf tube (static-Epp) an additional static air–water interface was present. Orbital shaking introduced hydrodynamic mixing effects in the agitated syringe (OShaking-Syr), whereas, in the case of agitated Eppendorf tube (OShaking-Epp), it provoked a combination of hydrodynamic flow and interfacial interaction with a moving air–water interface. In the simulated microgravity environment, the sample sealed in the syringe (microgravity-Syr) experienced less sedimentation compared with the static condition. Whereas the protein solution under microgravity in an Eppendorf tube (microgravity-Epp) was exposed to a continuous 3D rotation of the air–water interface.

Nanoscale imaging of α-synuclein amyloid formation

To unravel the process of protein fibrillization at the single aggregate scale, we used high-resolution AFM imaging of the 3D morphology of individual protein assemblies (Fig. 2). To improve adsorption of the negatively charged α-synuclein species on the surface, we exploited the positive chemical functionalization of mica by APTES. For each of the conditions shown in Fig. 1, we collected an aliquot of the aggregating solution after 4, 8, 12, 16 and 30 days of incubation, which were then deposited on the positive functionalized mica. This

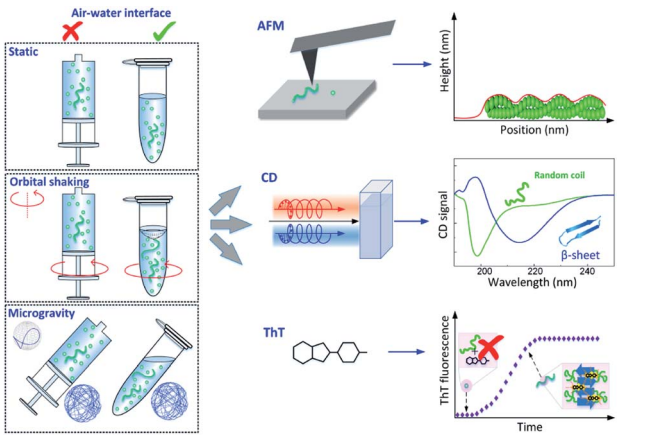

Fig. 1 Schematic of the experimental approach. Left: the time course of α-synuclein aggregation was studied under a combination of distinct dynamic conditions (static, orbital shaking and microgravity[40]) and in the presence or absence of an air–water interface, as implemented in Eppendorf tubes or syringes respectively. Right: experimental methods used to characterize α-synuclein aggregates and aggregation kinetics: high-resolution AFM microscopy to assess aggregates morphology and formation (Top), CD spectroscopy to investigate changes in secondary structure (Middle), and ThT fluorescence assay to study aggregation kinetics (Bottom).

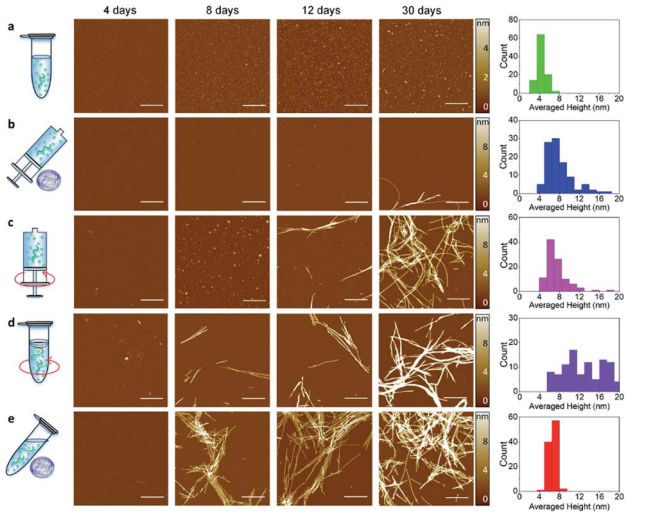

Fig. 2 High-resolution imaging of amyloid fibrils formation by AFM. Time points of aggregation at 4, 8, 12, 16 and 30 days in static-Eppendorf (static-Epp) (a), microgravity-Syringe (microgravity-Syr) (b), Orbital Shaking-Syringe (OShaking-Syr) (c), Orbital Shaking-Eppendorf (OShaking-Epp) (d) and microgravity-Eppendorf (microgravity-Epp) (e) conditions at initial monomeric concentration of 45 μM. Scale bar is 1 μm. The histograms (right) show the statistical distribution of the cross-sectional height (Fig. S2†) of fibrillar aggregates after 30 days.

approach enabled to monitor the process of aggregation at high spatial resolution and at the single aggregate level.

A qualitative observation of the aggregation in each condition of incubation demonstrates that protein aggregated slower in static and microgravity syringe conditions. In static conditions in both the absence and presence of an air–water interface only very few and short protofibrils with typical fibril cross-sectional diameter (Fig. S1†) of 4 ± 2 nm were formed after 30 days (Fig. 2a). The formation of mature amyloid fibrils occurred both in the presence and in the absence of an air–water interface only after 54 days (Fig. S2†). Remarkably, in static conditions, the presence of the air–water interface did not significantly affect the process of amyloid formation. In microgravity-Syr conditions, mature fibrillar aggregates with cross-sectional diameter above 6 nm were observed already after 16 days, they increased in abundance after 30 days incubation, and the formation of abundant mature amyloid fibrils was observed after 54 days (Fig. S2†). In contrast, OShaking-Epp conditions lead to the formation of abundant mature fibrillar aggregates after only 16 days of incubation. In the presence of a moving air–water interface (OShaking-Epp and microgravity-Epp), abundant mature fibrillar aggregates were formed already after 8 days of incubation. These aggregates had typical lengths of few micrometers and a cross-sectional height above 6 nm.

We confirmed these observations by measuring quantitatively the volume of fibrillar aggregates formed at different time points under each condition (Fig. S3†). After 30 days of incubation, less fibrillar mass was formed under static and microgravity-Syr conditions in comparison to all other incubation conditions. In both static conditions, *i.e.* irrespective of the presence or absence of an air–water interface, we observed a similar speed of aggregation and similar amounts of fibrils formed (Fig. S4†). After 54 days of incubation, a similar volume of fibrillar aggregates was produced in all conditions (Fig. S3†). The data indicates that sedimentation has the capability to slower the aggregation kinetics and that reduced sedimentation effects in a microgravity environment slightly increases the speed of amyloid formation. Moreover, we observed that the amyloid fibrils formed in each condition showed a high degree of polymorphism (Fig. S5 and S6†).

Correlation of CD spectroscopy and ThT fluorescence to characterize aggregation

CD spectroscopy was used to monitor the secondary structural transition from the disordered native form of monomeric α-synuclein to the amyloid cross-β sheet conformation. Random coil and cross-β sheet show typical absorptions at 198 nm and 220 nm, respectively (Fig. 1). In all the experimental conditions studied in the present work, aliquots of the aggregation reaction were collected to acquire CD spectra as a function of the incubation time. The CD spectra recorded at a concentration of 45 μM are shown in Fig. 3 left and Fig. S7.† For all the studied conditions, the gradual shift of the minimum of the CD spectrum at 198 nm to 220 nm indicated the formation of cross-β sheet conformation as a function of the incubation time.

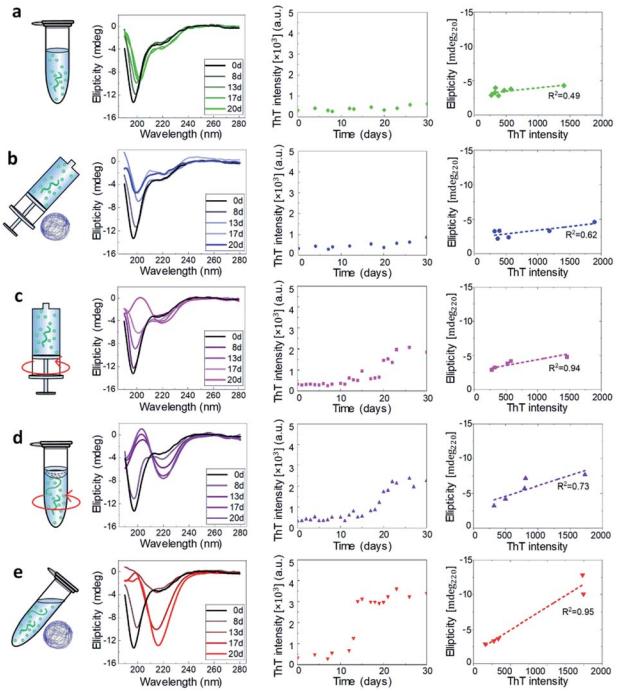

Fig. 3 CD and ThT characterization of α-synuclein aggregation at 45 μM. For each experimental condition defined in Fig. 1, we show as a function of the incubation time the CD spectra (Left), the ThT assay (Middle) and the correlation at each time point between ThT intensity and CD signal at 220 nm (Right). The dashed lines are the best linear fits to the scattering plots.

The ThT dye shows a specific fluorescence signal upon binding to cross-β sheet aggregates,[40,41] and can be used to monitor the aggregation kinetics of α-synuclein. We studied the aggregation process at the initial monomeric concentrations of 20, 30, 45, 55, 60 μM (Fig. 3 and S8†).

In each condition defined in our work, we then quantitatively evaluated the propensity of α-synuclein to form cross-β sheet amyloid fibrils as a function of the incubation time by correlating at each time point the increase of ThT fluorescence *versus* the structural change measured at 220 nm (Fig. S9†).[34,42] In Fig. 3 middle, the kinetic curves of aggregation in each condition at 45 μM are presented. A steeper curve indicates faster kinetics of aggregation. Then, in Fig. 3 right, we show a plot of the intensity of ThT fluorescence *versus* the absolute value of CD intensity, where the slope of the linear fitting of the ThT *vs.* CD data was used to characterize the tendency to form cross-β sheet fibrillar protein (Fig. 4a and b).

The data indicated that the kinetics of aggregation and structural transition to fibrillar amyloid cross-β sheet of α-synuclein in static (static-Epp and static-Syr) and microgravity-Syr conditions are significantly slower than the kinetics of aggregation in the presence of strong hydrodynamic mixing and a moving (OShaking-Epp) and 3D rotating (microgravity-Epp) air–water interface. Aggregation of α-synuclein under OShaking-Epp conditions showed intermediate kinetics of aggregation and cross-β sheet formation. The spectroscopic and kinetic data were in excellent agreement with the AFM

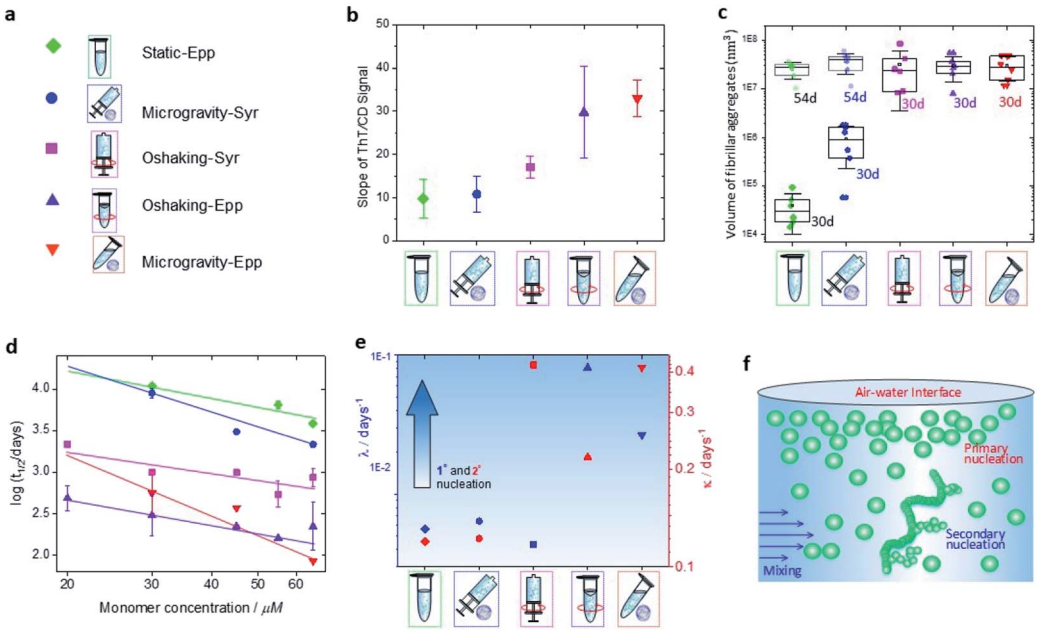

Fig. 4 Effects of environmental stimuli on α-synuclein microscopic steps of aggregation. (a) Legend of the condition of incubation used in the present work. (b) Slope of the ThT *vs.*, CD signal at 45 μM. (c) Volume of the fibrillar aggregates formed under incubation in each condition after 30 days (solid points) and 54 days (transparent points). (d) A double logarithmic plot of the half time of aggregation *versus* initial protein concentration. (e) Rates of primary nucleation (blue) and secondary (red) processes at 30 μM monomer concentration obtained from global fitting of the aggregation kinetics at the different conditions to an integrated rate law. (f) Schematic representation of the effect of hydrodynamic mixing and air–water interface on primary nucleation and secondary process during aggregation of α-synuclein. Primary nucleation is significantly increased in the presence of a moving air–water interface, whereas secondary processes are increased by rotating in the presence of an air–water interface or shaking.

quantification of the volume of formed fibrillar aggregates as measured by AFM as a function of the incubation time (Fig. 4c and S10†). The described trends of relative aggregation rates were also reflected in the aggregation half-times $t_{1/2}$ measured in the ThT assays (Fig. 4d). Interestingly, reduced gravitational effects seemed to alter the concentration dependence of the relative overall aggregation rate as compared to ambient conditions. This indicated that the different experimental conditions tested influence the aggregation of α-synuclein in a complex manner, likely effecting more than one microscopic step.

Chemical kinetics analysis

We have established that the different experimental conditions tested affect the overall rate of aggregation of α-synuclein in distinct ways. To understand the origin of these effects, a chemical kinetics analysis was performed (Fig. S11–S14†). The underlying principle of this analysis is to map the differences in the aggregation curves to changes in the rate constants of the individual microscopic steps. For α-synuclein, the reaction network of microscopic steps consists of primary nucleation, *i.e.* the spontaneous formation of new aggregates, growth or elongation of existing fibrils and secondary processes, in which existing aggregates facilitate the formation of additional fibrils.[38,43,44] The rate constants and rates of each microscopic step can be obtained from global fitting of a measurement of the aggregate concentration over time, as recorded in ThT assays, to an integrated rate law (ESI†).[37,45] In Fig. 4e, the rates of primary nucleation, λ, and secondary processes, κ, are plotted against the tested experimental conditions. Sedimentation effects, as probed by the microgravity-Syr condition, did not significantly affect the rates of primary nucleation or secondary processes of α-synuclein as compared to the reference, static-Epp. We found that primary nucleation was significantly increased in the presence of a moving air–water interface (OShaking-Epp and microgravity-Epp). This result is consistent with previous studies of the interactions between α-synuclein aggregates and hydrophobic interfaces such as lipid membranes.[43,46] A plausible explanation is the accumulation of monomeric proteins onto the air–water interface due to interactions with hydrophobic protein domains.[25,47,48] Secondary processes, on the other hand, were facilitated by rotating in the presence of an air–water interface or shaking. This indicates that agitation promotes secondary processes, but the accelerating effect differs with the agitation approach, *i.e.* with the type of the hydrodynamic flow field and its intensity.[14,18]

Conclusions

In summary, we present a comprehensive study that explores the influence of several environmental factors on α-synuclein aggregation, including microgravity-induced under-sedimentation, hydrodynamic mixing and interactions of the air–water interface. Our results reveal that microgravity-induced

under-sedimentation shows minor differences when compared to slow aggregation in static conditions, independent of the presence of a static air–water interface. Inhibition of sedimentation by microgravity results in only a slight promotion of aggregation and mature fibril formation, which is consistent with previous reports,[31,49,50] but it exhibits no significant difference on the rates of primary nucleation nor secondary processes. Hydrodynamic mixing highly promotes the formation of amyloid fibrils, both in the presence and absence of an air–water interface. Under orbital shaking and in the absence of an air–water interface, the presence of hydrodynamic mixing increases the rate of secondary process during the aggregation, an effect that has been observed for other amyloid forming systems and was there attributed to increased fragmentation.[51] In the presence of a moving air–water interface, a further increase of the rate of primary nucleation is observed, that agrees with previous literature,[14] as shown in Fig. 4e and f. This increased rate of primary nucleation may be a result of the interaction of monomeric proteins at the air–water interface.

Overall, these observations enrich the understanding of the influence of environmental stimuli on the microscopic steps determining the phenomenon of α-synuclein amyloid formation. Environmental factors are not only critical in promoting fibril formation, but are of great importance for the comprehension of α-synuclein aggregation and amyloid formation, which is fundamental for attempting high-throughput assays and seeking pharmacological treatments for Parkinson's disease.

Experimental

Expression and purification of α-synuclein

Recombinant wild type α-synuclein was expressed by *E. coli* and then purified as described previously.[52]

Experimental setup and aggregation assay

Purified monomeric α-synuclein protein was dissolved in buffer (50 mM Tris HCl, 150 mM NaCl, pH 7.4), and filtered through a 100 kDa filter. The α-synuclein concentration in the solution was determined by ultraviolet absorbance (Nanodrop 2000). An aliquot (1 mL) of α-synuclein solution was sealed either in a low protein-binding syringe while gently removing the gas vesicle inside or in an Eppendorf tube. The α-synuclein solution was incubated at 37 °C in static, orbital shaking, and RPM-induced microgravity conditions.

In static condition, the protein solution samples were statically incubated in the incubator at 37 °C. In orbital shaking condition, the α-synuclein solutions in both the Eppendorf tube and the syringe were vertically fixed and agitated in the horizontal plane at the speed of 400 rpm. The microgravity environment was simulated by using a self-build random position machine (RPM) with the reported protocol.[29] This RPM system was realized by employing 3D-clinostat configuration[53–55] to rotate three-dimensionally the sample with well-controlled speed and acceleration. This RPM system contains two independent high-precision motors to give a random rotation orientation and gravity vector on the sample, providing a simulated microgravity condition for protein aggregation. For the condition of microgravity, the α-synuclein solution was sealed in the syringe and incubated in the chamber of the RPM system at 37 °C. The sample solutions were placed in the rotational center of the RPM system to maintain an average null gravity vector and to minimize residual gravity artifacts during the experiment.[29,56] Due to the size of the syringe used, the protein samples experienced a free-fall with small spherical trajectories, resulting in a good approximation of a microgravity environment ranging from 0 g to 0.2 g.[29,39] During the experiment, a constant speed of ~30 rpm was applied on both axes. This relatively fast speed was chosen to generate the simulated microgravity and to maintain the centrifugal force minimal. For the 3-dimentional (3D) shaking condition, the α-synuclein solutions in the Eppendorf tube were also incubated in the RPM system. However, instead of generating microgravity, the agitation in random direction generated 3-dimensional liquid turbulence in the Eppendorf tube. This effect provoked the influence of hydrodynamic mixing and interaction between protein and air–water interface, on the protein aggregation in the bulk solution in the Eppendorf tube.

AFM measurement

An aliquot (10 μL) of diluted α-synuclein solution (10 μM) was prepared before each AFM measurement. Freshly cleaved mica was functionalized with an aliquot (10 μL) of 0.5% (3-aminopropyl) triethoxysilane (APTES) for 1.5 min at room temperature, and was then rinsed and dried with a compressed gas flow. Then, an aliquot (10 μL) of the α-synuclein solution with a concentration of 10 μM was deposited on the functionalized mica for 4 min, which was immediately rinsed with Milli-Q water and dried by a gentle flow of nitrogen gas. AFM imaging was operated by Park NX10 AFM (Park Systems, South Korea) in non-contact mode in ambient conditions. PPP-NCHR cantilevers (Park Systems, South Korea) were used, they have a typical spring constant of 42 N m^{-1} and a tip radius of less than 7 nm. A stable and weak tip–sample interaction was applied during scanning with a phase variation of ±5° in the negative region for a consistent measurement of fibrillar cross-sectional dimensions.[36] AFM images were flattened using XEI software (Park Systems, South Korea). The statistical analysis of amyloid fibrils on the AFM images was carried out by SPIP software (Image Metrology, Denmark). The average height of amyloid fibrils was measured by averaging the cross section of the fibrillar structure. More than 100 fibrils on multiple random scanned locations were measured in each condition. The volume of fibrils was characterized by using SPIP software and compared between the fibrils from different 4 × 4 $μm^2$ AFM images and six random-selected areas were calculated in each condition.

CD spectroscopy

An aliquot (40 μL) of diluted α-synuclein solution (15 μM) was analyzed with a Jasco J-815 CD spectrometer in the range of 190–280 nm in each measurement at room temperature. A high-quality quartz cuvette with an optical path length of 1.0 mm

was employed and spectra were collected every 0.2 nm in continuous scanning mode at a speed of 40 nm min^{-1}. Further smoothing of spectra was processed with a Savitzky–Golay filter (10 points, 2nd order).

ThT fluorescence assay

Fresh ThT solution was prepared from stock solution before each measurement at a concentration of 100 μM. An aliquot of α-synuclein solution was diluted by ThT solution and Milli-Q water to reach a final concentration of 3 μM and a ThT concentration of 10 μM in every experiment. An aliquot of prepared α-synuclein solution (70 μL) in each conditions was measured in a Bucher Analyst AD plate reader. ThT measurements were performed at an excitation wavelength of 450 nm and an emission wavelength of 485 nm.

Quantitative analysis of ThT assays

The ThT assays were analyzed using the online fitting software AmyloFit, following the referred guidelines.[37] In summary, the normalized data were fitted to the general model 'secondary nucleation dominated, unseeded'. Each fitting parameter was constraint to have identical values for a given experimental condition. The fitted lines are shown in Fig. S11.† The fitting results were converted into the rate of primary nucleation, λ, and secondary processes, κ, according to

$$\lambda = \sqrt{2k + k_n m_0^{n_c}}$$

and

$$\kappa = \sqrt{2k + k_2 m_0^{(n_2+1)}}$$

respectively, where the parameters $k + k_n$, n_c, $k + k_2$ and n_2 were obtained from fitting. The values for the intermediate concentration of 30 μM are plotted in Fig. 4e in the main text. The half-times shown in Fig. 4d in the main text were extracted from the normalized curves of the ThT assays using the 'Half Time Plotter' functionality of AmyloFit.

Conflicts of interest

There are no conflicts to declare.

Acknowledgements

We thank Christian Heinis and Xudong Kong from Laboratory of therapeutic proteins and peptides (LPPT), Hilal Lashuel from Laboratory of Molecular and Chemical Biology of Neurodegeneration (LMNN) for access to facilities. We acknowledge the support from the Swiss National Science Foundation Grants 200021_162767, the Herschel Smith Foundation (MRZ), and the Ramon Jenkins Fellowship of Sidney Sussex College (GM).

References

1 F. Chiti and C. M. Dobson, *Annu. Rev. Biochem.*, 2006, **75**, 333–366.
2 D. M. Christopher, *Nature*, 2003, **426**, 884.
3 T. P. J. Knowles, M. Vendruscolo and C. M. Dobson, *Nat. Rev. Mol. Cell Biol.*, 2014, **15**, 384.
4 G. Fusco, S. W. Chen, P. T. F. Williamson, R. Cascella, M. Perni, J. A. Jarvis, C. Cecchi, M. Vendruscolo, F. Chiti, N. Cremades, L. Ying, C. M. Dobson and A. D. Simone, *Science*, 2017, **358**, 1440–1443.
5 J. A. Rodriguez, M. I. Ivanova, M. R. Sawaya, D. Cascio, F. E. Reyes, D. Shi, S. Sangwan, E. L. Guenther, L. M. Johnson, M. Zhang, L. Jiang, M. A. Arbing, B. L. Nannenga, J. Hattne, J. Whitelegge, A. S. Brewster, M. Messerschmidt, S. Boutet, N. K. Sauter, T. Gonen and D. S. Eisenberg, *Nature*, 2015, **525**, 486–490.
6 J. Lautenschläger, A. D. Stephens, G. Fusco, F. Ströhl, N. Curry, M. Zacharopoulou, C. H. Michel, R. Laine, N. Nespovitaya, M. Fantham, D. Pinotsi, W. Zago, P. Fraser, A. Tandon, P. S. George-Hyslop, E. Rees, J. J. Phillips, A. D. Simone, C. F. Kaminski and G. S. K. Schierle, *Nat. Commun.*, 2018, **9**, 712.
7 F. S. Ruggeri, J. Adamcik, J. S. Jeong, H. A. Lashuel, R. Mezzenga and G. Dietler, *Angew. Chem.*, 2015, **127**, 2492–2496.
8 F. S. Ruggeri, F. Benedetti, T. P. J. Knowles, H. A. Lashuel, S. Sekatskii and G. Dietler, *Proc. Natl. Acad. Sci. U. S. A.*, 2018, **115**, 7230–7235.
9 L. Nielsen, R. Khurana, A. Coats, S. Frokjaer, J. Brange, S. Vyas, V. N. Uversky and A. L. Fink, *Biochemistry*, 2001, **40**, 6036–6046.
10 I. B. Bekard, P. Asimakis, J. Bertolini and D. E. Dunstan, *Biopolymers*, 2011, **95**, 733–745.
11 J. Adamcik and R. Mezzenga, *Soft Matter*, 2011, **7**, 5437.
12 M.-B. Fares, B. Maco, A. Oueslati, E. Rockenstein, N. Ninkina, V. L. Buchman, E. Masliah and H. A. Lashuel, *Proc. Natl. Acad. Sci. U. S. A.*, 2016, **113**, E912–E921.
13 S. M. Deguire, F. S. Ruggeri, M.-B. Fares, A. Chiki, U. Cendrowska, G. Dietler and H. A. Lashuel, *bioRxiv*, 2018, 358234.
14 F. Grigolato, C. Colombo, R. Ferrari, L. Rezabkova and P. Arosio, *ACS Nano*, 2017, **11**, 11358–11367.
15 J. Habchi, S. Chia, C. Galvagnion, T. C. T. Michaels, M. M. J. Bellaiche, F. S. Ruggeri, M. Sanguanini, I. Idini, J. R. Kumita, E. Sparr, S. Linse, C. M. Dobson, T. P. J. Knowles and M. Vendruscolo, *Nat. Chem.*, 2018, **10**, 673–683.
16 A. Tiiman, A. Noormägi, M. Friedemann, J. Krishtal, P. Palumaa and V. Tõugu, *J. Pept. Sci.*, 2013, **19**, 386–391.
17 C. F. Lee, S. Bird, M. Shaw, L. Jean and D. J. Vaux, *J. Biol. Chem.*, 2012, **287**, 38006–38019.
18 J. Dobson, A. Kumar, L. F. Willis, R. Tuma, D. R. Higazi, R. Turner, D. C. Lowe, A. E. Ashcroft, S. E. Radford, N. Kapur and D. J. Brockwell, *Proc. Natl. Acad. Sci. U. S. A.*, 2017, 201702724.
19 K. M. Batzli and B. J. Love, *Mater. Sci. Eng. Carbon*, 2015, **48**, 359–364.
20 M. Manno, D. Giacomazza, J. Newman, V. Martorana and P. L. San Biagio, *Langmuir*, 2010, **26**, 1424–1426.

21 S. Campioni, G. Carret, S. Jordens, L. Nicoud, R. Mezzenga and R. Riek, *J. Am. Chem. Soc.*, 2014, **136**, 2866–2875.
22 N. A. Bernhardt, W. M. Berhanu and U. H. E. Hansmann, *J. Phys. Chem. B*, 2013, **117**, 16076–16085.
23 Z. Liao, J. W. Lampe, P. S. Ayyaswamy, D. M. Eckmann and I. J. Dmochowski, *Langmuir*, 2011, **27**, 12775–12781.
24 Y. Song, U. Shimanovich, T. C. T. Michaels, Q. Ma, J. Li, T. P. J. Knowles and H. C. Shum, *Nat. Commun.*, 2016, **7**, 12934.
25 S. Jordens, E. E. Riley, I. Usov, L. Isa, P. D. Olmsted and R. Mezzenga, *ACS Nano*, 2014, **8**, 11071–11079.
26 S. L. Wuest, B. Gantenbein, F. Ille and M. Egli, *npj Microgravity*, 2018, **4**, 7.
27 M. Sieber, W. Hanke and F. P. M. Kohn, *Open J. Biophys.*, 2014, **4**, 105.
28 M. Sieber, S. Kaltenbach, W. Hanke and F. P. M. Kohn, *J. Biomed. Sci. Eng.*, 2016, **9**, 361.
29 S. Dinarelli, G. Longo, G. Dietler, A. Francioso, L. Mosca, G. Pannitteri, G. Boumis, A. Bellelli and M. Girasole, *Sci. Rep.*, 2018, **8**, 1–12.
30 M. Goldermann and W. Hanke, *Microgravity Sci. Technol.*, 2001, **13**, 35.
31 Y. Takamatsu, W. Koike, T. Takenouchi, S. Sugama, J. Wei, M. Waragai, K. Sekiyama and M. Hashimoto, *npj Microgravity*, 2016, **2**, 16013.
32 D. Bell, S. Durrance, D. Kirk, H. Gutierrez, D. Woodard, J. Avendano, J. Sargent, C. Leite, B. Saldana, T. Melles, S. Jackson and S. Xu, *Gravitational and Space Research*, 2018, vol. 6, pp. 10–26.
33 F. S. Ruggeri, J. Habchi, A. Cerreta and G. Dietler, *Curr. Pharm. Des.*, 2016, **22**, 3950–3970.
34 M. Perni, C. Galvagnion, A. Maltsev, G. Meisl, M. B. D. Müller, P. K. Challa, J. B. Kirkegaard, P. Flagmeier, S. I. A. Cohen, R. Cascella, S. W. Chen, R. Limboker, P. Sormanni, G. T. Heller, F. A. Aprile, N. Cremades, C. Cecchi, F. Chiti, E. A. A. Nollen, T. P. J. Knowles, M. Vendruscolo, A. Bax, M. Zasloff and C. M. Dobson, *Proc. Natl. Acad. Sci. U. S. A.*, 2017, **114**, E1009–E1017.
35 F. S. Ruggeri, T. Šneideris, M. Vendruscolo and T. P. J. Knowles, *Arch. Biochem. Biophys.*, 2019, **664**, 134–148.
36 F. S. Ruggeri, S. Vieweg, U. Cendrowska, G. Longo, A. Chiki, H. A. Lashuel and G. Dietler, *Sci. Rep.*, 2016, **6**, 31155.
37 G. Meisl, J. B. Kirkegaard, P. Arosio, T. C. T. Michaels, M. Vendruscolo, C. M. Dobson, S. Linse and T. P. J. Knowles, *Nat. Protoc.*, 2016, **11**, 252–272.
38 T. P. J. Knowles, C. A. Waudby, G. L. Devlin, S. I. A. Cohen, A. Aguzzi, M. Vendruscolo, E. M. Terentjev, M. E. Welland and C. M. Dobson, *Science*, 2009, **326**, 1533–1537.
39 S. L. Wuest, S. Richard, S. Kopp, D. Grimm and M. Egli, *BioMed Res. Int.*, 2015, **2015**, 971474.
40 J. Pronchik, X. He, J. T. Giurleo and D. S. Talaga, *J. Am. Chem. Soc.*, 2010, **132**, 9797–9803.
41 P. Arosio, T. P. J. Knowles and S. Linse, *Phys. Chem. Chem. Phys.*, 2015, **17**, 7606–7618.
42 H.-L. Zhu, S.-R. Meng, J.-B. Fan, J. Chen and Y. Liang, *PLoS One*, 2011, **6**, e25020.
43 C. Galvagnion, A. K. Buell, G. Meisl, T. C. T. Michaels, M. Vendruscolo, T. P. J. Knowles and C. M. Dobson, *Nat. Chem. Biol.*, 2015, **11**, 229–234.
44 M. Iljina, A. J. Dear, G. A. Garcia, S. De, L. Tosatto, P. Flagmeier, D. R. Whiten, T. C. T. Michaels, D. Frenkel, C. M. Dobson, T. P. J. Knowles and D. Klenerman, *ACS Nano*, 2018, **12**, 10855–10866.
45 G. Meisl, T. C. T. Michaels, S. Linse and T. P. J. Knowles, in *Amyloid Proteins*, Humana Press, New York, NY, 2018, pp. 181–196.
46 J. W. P. Brown, A. K. Buell, T. C. T. Michaels, G. Meisl, J. Carozza, P. Flagmeier, M. Vendruscolo, T. P. J. Knowles, C. M. Dobson and C. Galvagnion, *Sci. Rep.*, 2016, **6**, 36010.
47 S. Rudiuk, L. Cohen-Tannoudji, S. Huille and C. Tribet, *Soft Matter*, 2012, **8**, 2651–2661.
48 M. Monica Castellanos, J. A. Pathak and R. H. Colby, *Soft Matter*, 2014, **10**, 122–131.
49 H. Cai, C. Wei-na, J. Sunggoan, R. Sarah, M. Stuart and M. Bronwen, *Curr. Alzheimer Res.*, 2012, **9**, 5–17.
50 R. Mayeux and Y. Stern, *Cold Spring Harbor Perspect. Med.*, 2012, **2**(8), a006239.
51 S. I. A. Cohen, S. Linse, L. M. Luheshi, E. Hellstrand, D. A. White, L. Rajah, D. E. Otzen, M. Vendruscolo, C. M. Dobson and T. P. J. Knowles, *Proc. Natl. Acad. Sci. U. S. A.*, 2013, **110**, 9758–9763.
52 W. Hoyer, T. Antony, D. Cherny, G. Heim, T. M. Jovin and V. Subramaniam, *J. Mol. Biol.*, 2002, **322**, 383–393.
53 A. Manzano, R. Herranz, L. A. den Toom, S. Te Slaa, G. Borst, M. Visser, F. J. Medina and J. J. W. A. van Loon, *npj Microgravity*, 2018, **4**, 1–11.
54 R. Herranz, R. Anken, J. Boonstra, M. Braun, P. C. M. Christianen, M. de Geest, J. Hauslage, R. Hilbig, R. J. A. Hill, M. Lebert, F. J. Medina, N. Vagt, O. Ullrich, J. J. W. A. van Loon and R. Hemmersbach, *Astrobiology*, 2012, **13**, 1–17.
55 J. Pietsch, A. Sickmann, G. Weber, J. Bauer, M. Egli, R. Wildgruber, M. Infanger and D. Grimm, *Proteomics*, 2011, **11**, 2095–2104.
56 J. J. W. A. van Loon, *Adv. Space Res.*, 2007, **39**, 1161–1165.